Proceedings of the
47th IEEE Conference on Decision and Control
Cancun, Mexico, Dec. 9-11, 2008

Underwater Glider Motion Control

Nina Mahmoudian and Craig Woolsey

Abstract— **This paper describes an underwater glider motion control system intended to enhance locomotive efficiency by reducing the energy expended by vehicle guidance. In previous work, the authors derived an approximate analytical expression for steady turning motion by applying regular perturbation theory to a realistic vehicle model. The analysis results suggested the use of a well-known time-optimal path planning procedure developed for the Dubins car, an often-used model of a wheeled mobile robot. For underwater gliders operating at their most efficient flight condition, time-optimal glide paths correspond to energy-optimal glide paths. Thus, an analytically informed strategy for energy-efficient locomotion is to generate sequences of steady wings-level and turning motions according to the Dubins path planning procedure. Because the turning motion results are only approximate, however, and to compensate for model and environmental uncertainty, one must incorporate feedback to ensure convergent path following. This paper describes the dynamic modelling of the complete multi-body control system and the development and numerical implementation of a motion control system. The control system can be combined with a higher level guidance strategy involving Dubins-like paths to achieve energy-efficient locomotion.**

I. INTRODUCTION

Underwater gliders are highly efficient, winged autonomous underwater vehicles (AUVs) which locomote by modulating their buoyancy and their attitude. Applications include long-term, basin-scale oceanographic sampling and littoral surveillance. The first generation of underwater gliders includes *Slocum* [13], *Seaglider* [4], and *Spray* [11]. These "legacy gliders" have proven their worth as efficient, long-distance, long-endurance ocean sampling platforms. They can be deployed for months and travel thousands of kilometers. The exceptional endurance of underwater gliders is due to their reliance on gravity (weight and buoyancy) for propulsion and attitude control. Our aim is to develop implementable, energy-efficient motion control strategies that further improve the inherent efficiency of these vehicles. Outcomes will include more intelligent behaviors for existing vehicles and improved design guidelines for future underwater gliders. Having already characterized the existence and stability of steady wings-level and turning motions [9], ongoing research focuses on exploiting the properties of these steady motions to obtain real-time, nearly energy-optimal motion planning and control. A complete multi-body vehicle dynamic model, which includes actuator magnitude and rate limits, is used to develop and validate a motion controller that can be used to obtain the (approximate) steady motions predicted by analysis. These steady motions can then be concatenated to achieve compatible guidance objectives, such as waypoint following. Section II develops a general dynamic model for an underwater glider. Section III reviews the conditions for wings-level gliding flight given in [6] and the approximate conditions for steady turning flight developed in [9]. In Section IV, it is recognized that the special structure of the approximate solution given in Section III suggests the use of existing optimal path planning results for planar mobile robots. The control design is presented in Section V. Simulation results for the *Slocum* model given in [1] are presented in Section VI. Conclusions and a description of ongoing research are provided in Section VII.

Department of Aerospace & Ocean Engineering, Virginia Tech, Blacksburg, VA 24061 {ninam, cwoolsey}@vt.edu

II. VEHICLE DYNAMIC MODEL

The glider is modeled as a rigid body (mass m_{rb}) with two moving mass actuators ($m_{\mathrm{p_x}}$ and $m_{\mathrm{p_y}}$) and a variable ballast actuator (m_{b}). The total vehicle mass is

$$m_{\mathrm{v}} = m_{\mathrm{rb}} + m_{\mathrm{p_x}} + m_{\mathrm{p_y}} + m_{\mathrm{b}},$$

where m_{b} can be modulated by control. The vehicle displaces a volume of fluid of mass m. Let $\tilde{m} = m_{\mathrm{v}} - m$. If $\tilde{m} > 0$, the vehicle is heavy in water and tends to sink while if If $\tilde{m} < 0$, the vehicle is buoyant in water and tends to rise. Figure 1 shows the simplified model for the underwater glider actuation system. The variable mass is represented by a mass particle m_{b} located at the origin of a body-fixed reference frame. The vehicle's attitude is given by a proper

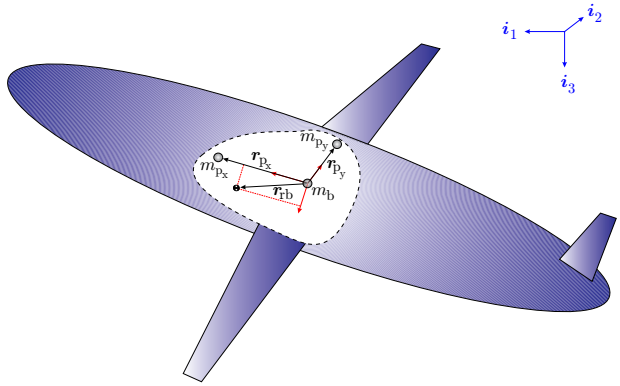

Fig. 1. Illustration of point mass actuators.

rotation matrix $\boldsymbol{R}_{\mathrm{IB}}$ which maps free vectors from the body-fixed reference frame to a reference frame fixed in inertial space. The body frame is defined by an orthonormal triad $\{\boldsymbol{b}_1, \boldsymbol{b}_2, \boldsymbol{b}_3\}$, where $\boldsymbol{b}_1$ is aligned with the body's longitudinal axis. The inertial frame is represented by an orthonormal triad $\{\boldsymbol{i}_1, \boldsymbol{i}_2, \boldsymbol{i}_3\}$, where $\boldsymbol{i}_3$ is aligned with the local direction of gravity. Following standard vehicle modeling convention,

we parameterize $\boldsymbol{R}_{\rm IB}$ with three Euler angles: the roll angle ϕ, the pitch angle θ, and the yaw angle ψ. To define the rotation matrix explicitly, let

$$\boldsymbol{e}_1 = \begin{pmatrix} 1 \\ 0 \\ 0 \end{pmatrix}, \quad \boldsymbol{e}_2 = \begin{pmatrix} 0 \\ 1 \\ 0 \end{pmatrix}, \quad \text{and} \quad \boldsymbol{e}_3 = \begin{pmatrix} 0 \\ 0 \\ 1 \end{pmatrix}$$

represent the standard basis for $\mathbb{R}^3$. Also, let the character $\hat{\cdot}$ denote the 3×3 skew-symmetric matrix satisfying $\hat{\boldsymbol{a}}\boldsymbol{b} = \boldsymbol{a} \times \boldsymbol{b}$ for 3-vectors $\boldsymbol{a}$ and $\boldsymbol{b}$. Then $\boldsymbol{R}_{\rm IB} = e^{\widehat{\boldsymbol{e}_3}\psi} e^{\widehat{\boldsymbol{e}_2}\theta} e^{\widehat{\boldsymbol{e}_1}\phi}$. Let $\boldsymbol{v} = [u,\ v,\ w]^T$ represent the translational velocity and let $\boldsymbol{\omega} = [p,\ q,\ r]^T$ represent the rotational velocity of the underwater glider with respect to inertial space, where $\boldsymbol{v}$ and $\boldsymbol{\omega}$ are both expressed in the body frame. If $\boldsymbol{x}$ represents the position of the body frame origin with respect to the inertial frame, the vehicle kinematic equations are

$$\begin{aligned} \dot{\boldsymbol{x}} &= \boldsymbol{R}_{\rm IB}\boldsymbol{v} && (1) \\ \dot{\boldsymbol{R}}_{\rm IB} &= \boldsymbol{R}_{\rm IB}\hat{\boldsymbol{\omega}}. && (2) \end{aligned}$$

The dynamic equations relate external forces and moments to rates of change of velocity. Accordingly, following [14], define the mass, inertia, and inertial coupling matrices for the combined rigid body/moving mass/variable ballast system as

$$\begin{aligned} \boldsymbol{I}_{\rm rb/p/b} &= \boldsymbol{I}_{\rm rb} - m_{\rm p_x}\hat{\boldsymbol{r}}_{\rm p_x}\hat{\boldsymbol{r}}_{\rm p_x} - m_{\rm p_y}\hat{\boldsymbol{r}}_{\rm p_y}\hat{\boldsymbol{r}}_{\rm p_y} \\ \boldsymbol{M}_{\rm rb/p/b} &= m_{\rm v}\mathbf{1} \\ \boldsymbol{C}_{\rm rb/p/b} &= m_{\rm rb}\hat{\boldsymbol{r}}_{\rm rb} + m_{\rm p_x}\hat{\boldsymbol{r}}_{\rm p_x} + m_{\rm p_y}\hat{\boldsymbol{r}}_{\rm p_y} \end{aligned}$$

where $\mathbf{1}$ represents the 3×3 identity matrix. As indicated in Figure 1, the mass particle $m_{\rm p_x}$ is constrained to move along the longitudinal axis while the mass particle $m_{\rm p_y}$ is constrained to move along the lateral axis:

$$\boldsymbol{r}_{\rm p_x} = r_{\rm p_x}\boldsymbol{e}_1 \quad \text{and} \quad \boldsymbol{r}_{\rm p_y} = r_{\rm p_y}\boldsymbol{e}_2.$$

The rigid body inertia matrix $\boldsymbol{I}_{\rm rb}$ represents the distribution of mass $m_{\rm rb}$. The added mass matrix $\boldsymbol{M}_{\rm f}$, the added inertia matrix $\boldsymbol{I}_{\rm f}$, and the added inertial coupling matrix $\boldsymbol{C}_{\rm f}$ account for the energy necessary to accelerate the fluid around the vehicle as it rotates and translates.It is notationally convenient to compile the various inertia matrices into the *generalized* inertia matrix shown in the table below, See [14].

Inertia $\mathbb{I}$			
$\boldsymbol{I}_{\rm rb/p/b} + \boldsymbol{I}_{\rm f}$	$\boldsymbol{C}_{\rm rb/p/b} + \boldsymbol{C}_{\rm f}$	$m_{\rm p_x}\hat{\boldsymbol{r}}_{\rm p_x}\boldsymbol{e}_1$	$m_{\rm p_y}\hat{\boldsymbol{r}}_{\rm p_y}\boldsymbol{e}_2$
$\boldsymbol{C}^T_{\rm rb/p/b} + \boldsymbol{C}^T_{\rm f}$	$\boldsymbol{M}_{\rm rb/p/b} + \boldsymbol{M}_{\rm f}$	$m_{\rm p_x}\boldsymbol{e}_1$	$m_{\rm p_y}\boldsymbol{e}_2$
$-m_{\rm p_x}\boldsymbol{e}_1^T\hat{\boldsymbol{r}}_{\rm p_x}$	$m_{\rm p_x}\boldsymbol{e}_1^T$	$m_{\rm p_x}$	0
$-m_{\rm p_y}\boldsymbol{e}_2^T\hat{\boldsymbol{r}}_{\rm p_y}$	$m_{\rm p_y}\boldsymbol{e}_2^T$	0	$m_{\rm p_y}$

Let $\boldsymbol{p}_{\rm sys}$ represent the total linear momentum of the vehicle/fluid system and let $\boldsymbol{h}_{\rm sys}$ represent the total angular momentum. Let $\boldsymbol{p}_{\rm p_x}$ and $\boldsymbol{p}_{\rm p_y}$ represent the total translational momentum of the moving mass particles, and let $p_{\rm p_x} = \boldsymbol{e}_1 \cdot \boldsymbol{p}_{\rm p_x}$ and $p_{\rm p_y} = \boldsymbol{e}_2 \cdot \boldsymbol{p}_{\rm p_x}$ represent their components along their respective axes of controlled motion. Defining the generalized velocity $\boldsymbol{\eta} = \begin{pmatrix} \boldsymbol{\omega}^T & \boldsymbol{v}^T & \dot{r}_{\rm p_x} & \dot{r}_{\rm p_y} \end{pmatrix}^T$ and the generalized momentum $\boldsymbol{\nu} = \begin{pmatrix} \boldsymbol{h}^T_{\rm sys} & \boldsymbol{p}^T_{\rm sys} & p_{\rm p_x} & p_{\rm p_y} \end{pmatrix}^T$, we have

$$\boldsymbol{\nu} = \mathbb{I}\boldsymbol{\eta} \qquad (3)$$

In writing the dynamic equations, it is convenient to define the "tilt" vector $\boldsymbol{\zeta} = \boldsymbol{R}^T_{\rm IB}\boldsymbol{i}_3$, which is simply the body frame unit vector pointing in the direction of gravity. The dynamic equations, with buoyancy control and moving mass actuator dynamics explicitly represented, are:

$$\begin{aligned} \dot{\boldsymbol{h}}_{\rm sys} &= \boldsymbol{h}_{\rm sys} \times \boldsymbol{\omega} + \boldsymbol{p}_{\rm sys} \times \boldsymbol{v} + \boldsymbol{T}_{\rm visc} \\ &\quad + (m_{\rm rb} g \boldsymbol{r}_{\rm rb} + m_{\rm p_x} g \boldsymbol{r}_{\rm p_x} + m_{\rm p_y} g \boldsymbol{r}_{\rm p_y}) \times \boldsymbol{\zeta} \\ \dot{\boldsymbol{p}}_{\rm sys} &= \boldsymbol{p}_{\rm sys} \times \boldsymbol{\omega} + \tilde{m} g \boldsymbol{\zeta} + \boldsymbol{F}_{\rm visc} \qquad (4) \\ \dot{\boldsymbol{\zeta}} &= \boldsymbol{\zeta} \times \boldsymbol{\omega} \\ \dot{p}_{\rm p_x} &= \boldsymbol{e}_1 \cdot (\boldsymbol{p}_{\rm p_x} \times \boldsymbol{\omega} + m_{\rm p_x} g \boldsymbol{\zeta}) + \tilde{u}_{\rm p_x} \\ \dot{p}_{\rm p_y} &= \boldsymbol{e}_2 \cdot \left(\boldsymbol{p}_{\rm p_y} \times \boldsymbol{\omega} + m_{\rm p_y} g \boldsymbol{\zeta}\right) + \tilde{u}_{\rm p_y} \\ \dot{m}_{\rm b} &= u_{\rm b} \end{aligned}$$

The forces $\tilde{u}_{\rm p_x}$ and $\tilde{u}_{\rm p_y}$ can be chosen to cancel the remaining terms in the equations for $\dot{p}_{\rm p_x}$ and $\dot{p}_{\rm p_y}$, so that

$$\begin{aligned} \dot{p}_{\rm p_x} &= u_{\rm p_x} \\ \dot{p}_{\rm p_y} &= u_{\rm p_y}. \end{aligned}$$

These inputs may then be chosen to servo-actuate the point mass positions for attitude control, although with inherent limits on point mass position and velocity. (Physically, these actuators might each consist of a large weight mounted on a lead screw that is driven by a servomotor.) The mass flow rate $u_{\rm b}$ is chosen to adjust the vehicle's net weight, again with inherent control magnitude and rate limits. These actuator limits are significant for underwater gliders and must be accounted for in control design and analysis.

The viscous forces and moments are expressed in terms of the hydrodynamic angles

$$\alpha = \arctan\left(\frac{w}{u}\right) \qquad \text{and} \qquad \beta = \arcsin\left(\frac{v}{V}\right)$$

where $V = \|\boldsymbol{v}\|$. Following standard modeling conventions,

$$\boldsymbol{F}_{\rm visc} = -e^{-\widehat{\boldsymbol{e}_2}\alpha} e^{\widehat{\boldsymbol{e}_3}\beta} \begin{pmatrix} \mathcal{D}(\alpha,\beta) \\ \mathcal{S}_\beta \beta + S_{\delta r}\delta r \\ \mathcal{L}_\alpha \alpha \end{pmatrix}$$

$$\boldsymbol{T}_{\rm visc} = \boldsymbol{D}_\omega \boldsymbol{\omega} + \begin{pmatrix} L_\beta \beta \\ M_\alpha \alpha \\ N_\beta \beta + N_{\delta r}\delta r \end{pmatrix}$$

The various coefficients, such as $\mathcal{L}_\alpha$ and N_β, depend on the vehicle's speed, its geometry, and the Reynolds number. The matrix $\boldsymbol{D}_\omega$ contains terms which characterize viscous angular damping (such as roll, pitch, and yaw rate damping). See [5], for example. Equations (4) are written in mixed velocity/momentum notation. To design a control system, we convert these into a consistent set of state variables by computing

$$\dot{\boldsymbol{\eta}} = \mathbb{I}^{-1}\dot{\boldsymbol{\nu}} - \mathbb{I}^{-1}\dot{\mathbb{I}}\ \ \mathbb{I}^{-1}\boldsymbol{\nu}. \qquad (5)$$

III. STEADY FLIGHT

In wings-level, gliding flight the vehicle has no angular velocity ($\boldsymbol{\omega} = \mathbf{0}$), no lateral velocity component ($v = 0$, so that $\beta = 0$), and no roll angle ($\phi = 0$). Also, $r_{\mathrm{p_y}} = 0$ and $\delta r = 0$ (if the vehicle has a rudder). Following the analysis presented in [6], one may compute the required CG location ($\boldsymbol{r}_{\mathrm{rb}}$) and the required net mass $\tilde{m}_0$ for balanced gliding flight at a specified speed and glide path angle. Let γ denote the glide path angle; in wings-level flight, $\gamma = \theta - \alpha$. For steady wings-level flight at a specified speed V_0 and glide path angle $\gamma_0 = \theta_0 - \alpha_0$,

$$\begin{aligned} \boldsymbol{r}_{\mathrm{rb}} &= \frac{1}{m_{\mathrm{rb}} g} \left(\boldsymbol{M}\boldsymbol{v}_0 \times \boldsymbol{v}_0 + \begin{pmatrix} 0 \\ M_\alpha \alpha_0 \\ 0 \end{pmatrix} \right) \times \boldsymbol{\zeta}_0 + \varrho \boldsymbol{\zeta}_0 \\ \tilde{m}_0 &= \frac{1}{g} \left(\cos(\gamma_0) \mathcal{L}_\alpha \alpha_0 - \sin(\gamma_0) \mathcal{D}(\alpha_0, 0) \right). \end{aligned}$$

In the equation for $\boldsymbol{r}_{\mathrm{rb}}$, $\boldsymbol{v}_0 = V_0 \left[\cos\alpha_0,\ 0,\ \sin\alpha_0\right]^T$, $\boldsymbol{\zeta}_0 = \left[-\sin\theta_0,\ 0,\ \cos\theta_0\right]^T$, and ϱ is a free parameter related to the vehicle's "bottom-heaviness" in the given flight condition [6]. (Note that, in determining a nominal wings-level glide condition, we assume that $r_{\mathrm{p_x}} = 0$. That is, the nominal gravitational moment is due entirely to $\boldsymbol{r}_{\mathrm{rb}}$.) Analysis of turning (helical) flight using a sophisticated underwater glider model is challenging. In [9], the problem was formulated as a regular perturbation problem in the turn rate, as represented by a small, non-dimensional turn rate parameter ϵ. In seeking a first order solution for turning flight, it was assumed that the pitch angle remains at its nominal value (θ_0) for wings-level flight. Polynomial expansions for $r_{\mathrm{p_y}}$, $\tilde{m}$, ϕ, V, α, and β in terms of ϵ were substituted into the nonlinear algebraic equations for steady turning flight. Solving the coefficient equation for ϵ^1 gives approximate equilibrium values for $r_{\mathrm{p_y}}$, $\tilde{m}$, ϕ, V, α, and β, to first order in ϵ. Letting the subscript 1 represent these first order approximate values, it was found in [9] that

$$\begin{aligned} V_1 &= 0 \\ \alpha_1 &= 0 \\ \tilde{m}_1 &= 0 \\ \beta_1 &= \beta_1(\alpha_0, \theta_0, \tilde{m}_0; \delta_{r_1}) \\ \phi_1 &= \phi_1(\alpha_0, \theta_0, \tilde{m}_0; \beta_1, \delta_{r_1}) \\ r_{\mathrm{p_{y_1}}} &= r_{\mathrm{p_{y_1}}}(\alpha_0, \theta_0, \tilde{m}_0; \delta_{r_1}) \end{aligned} \tag{6}$$

Equations (6) represent the first order approximate conditions for steady turning motion. Details, including explicit expressions for β_1, ϕ_1, and $r_{\mathrm{p_{y_1}}}$ as derived for a realistic vehicle model, are given in [9]. To assess stability of the true steady turning motion, one may linearize about the approximate equilibrium conditions and compute the eigenvalues of the state matrix. Because these eigenvalues depend continuously on the matrix parameters, stability of the true equilibrium may be inferred from stability of the approximate equilibrium provided (i) the equilibrium is hyperbolic and (ii) ϵ is small relative to the magnitude of the real part of each eigenvalue. (See Section 1.7 of [7] for a brief discussion and further references.) The approximate solution indicated in (6) shows that V, α, and $\tilde{m}$ remain constant to first order in ϵ. This suggests that the primary contributors to steady turning motion are lateral mass deflections ($r_{\mathrm{p_y}}$) and rudder deflections (δr) and that these deflections have no first order effect on speed or angle of attack. This is fortunate; in practice, it is considerably more costly to change the vehicle's net mass $\tilde{m}$ than to shift its CG. As discussed in the next section, these observations suggest a natural approach to path planning for underwater gliders.

IV. PATH PLANNING

With approximate analytical expressions for wings-level and turning flight in hand, a logical next step is to develop a procedure for planning efficient paths which makes use of these results. A reasonable objective is to concatenate the approximate equilibrium motions in order to minimize the time of transit from a given initial point to a given final point with a specified initial and final heading. A fortunate consequence of the structure indicated in (6) is that, to first order in turn rate, the horizontal and vertical components of velocity remain constant. Projecting the vehicle's motion onto the horizontal plane, glider equilibrium motions correspond to constant-speed straight and circular paths. So, to first order in turn rate, the minimum time control problem is equivalent to the Dubins car problem [12], [3]. The minimum time control policy is the concatenation of three motions: a left or right turn at maximum rate, a straight transit or a second turn at maximum rate, and a final turn at maximum rate. The optimal path can be determined through simple geometry, making it easily implementable in real-time control applications. For an underwater glider flying at maximum efficiency, this minimum time "Dubins path" corresponds to a minimum change in depth. Since an underwater glider propels itself using the force of gravity, minimizing the change in depth (potential energy) is equivalent to minimizing the energy expenditure. This is another appealing feature of Dubins paths, given that underwater gliders are specifically designed for locomotive efficiency.

V. CONTROL DESIGN

The vehicle guidance and control system is depicted conceptually in Figure 2, where the vector field $\boldsymbol{f}(\boldsymbol{x}, \boldsymbol{u})$ represents the system dynamics, and the vector field $\tilde{\boldsymbol{f}}(\boldsymbol{x}, \boldsymbol{u})$ notionally represents their first order approximation in turn rate. The block at the upper left in Figure 2 takes a commanded speed, glide path angle and turn rate and generates the corresponding equilibrium values of $\tilde{m}$, $r_{\mathrm{p_x}}$ and $r_{\mathrm{p_y}}$, as predicted by perturbation analysis. Because these values are only approximate, though, and because of modeling and environmental uncertainty, the commanded values of $\tilde{m}$, $r_{\mathrm{p_x}}$ and $r_{\mathrm{p_y}}$ are augmented using feedback compensation. This section focuses on the design of the feedback compensator.

A. Servo Controller Design

In designing the control system, it is convenient to replace the velocity $\boldsymbol{v}$, as expressed in the body reference frame, with

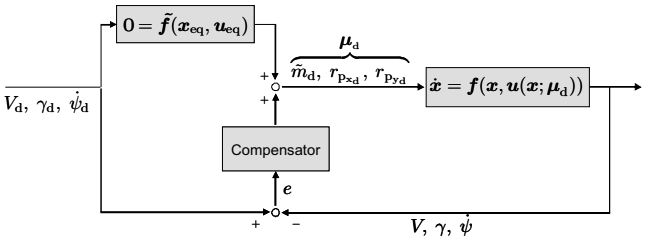

Fig. 2. The speed/glide path angle/turn rate control system.

speed, angle of attack, and sideslip angle (V, α, β). Thus,

$$\begin{aligned} \boldsymbol{v} &= e^{-\widehat{\boldsymbol{e}_2}\alpha} e^{\widehat{\boldsymbol{e}_3}\beta} (V\boldsymbol{e}_1) \\ \dot{\boldsymbol{v}} &= e^{-\widehat{\boldsymbol{e}_2}\alpha} e^{\widehat{\boldsymbol{e}_3}\beta} \begin{pmatrix} 1 & 0 & 0 \\ 0 & 0 & V \\ 0 & V\cos\beta & 0 \end{pmatrix} \begin{pmatrix} \dot{V} \\ \dot{\alpha} \\ \dot{\beta} \end{pmatrix}. \end{aligned}$$

The change of variables is well-defined for $\beta \in (-\frac{\pi}{2}, \frac{\pi}{2})$. Define the system state and control vectors

$$\begin{aligned} \mathbb{X} &= \left[\phi, \theta, V, \alpha, \beta, p, q, r, r_{\mathrm{p_x}}, v_{\mathrm{p_x}}, r_{\mathrm{p_y}}, v_{\mathrm{p_y}}\right]^T \\ \mathbb{U} &= \left[u_{\mathrm{p_x}}, u_{\mathrm{p_y}}, u_{\mathrm{b}}\right]^T \end{aligned}$$

The equations of motion can then be written in the form

$$\mathbb{F}(\dot{\mathbb{X}}, \mathbb{X}, \mathbb{U}) = \mathbf{0}$$

To design a servo-controller for the moving mass actuators and the variable ballast actuator, we linearize the dynamic equations and compute the transfer function for the input-output channel of interest. Let U denote one of the available input signals $U \in \left\{u_{\mathrm{p_x}}, u_{\mathrm{p_y}}, u_{\mathrm{b}}\right\}$ and define a corresponding output $Y(\mathbb{X})$. With these definitions, we obtain the perturbation equations

$$\triangle\dot{\mathbb{X}} = \boldsymbol{A}\triangle\mathbb{X} + \boldsymbol{B}\triangle U \quad (7)$$

$$\triangle Y = \boldsymbol{C}\triangle\mathbb{X} \quad (8)$$

where

$$\begin{aligned} \boldsymbol{A} &= -\left[\left(\frac{\partial\mathbb{F}}{\partial\dot{\mathbb{X}}}\right)^{-1}\left(\frac{\partial\mathbb{F}}{\partial\mathbb{X}}\right)\right]_{\mathrm{eq}} \\ \boldsymbol{B} &= -\left[\left(\frac{\partial\mathbb{F}}{\partial\dot{\mathbb{X}}}\right)^{-1}\left(\frac{\partial\mathbb{F}}{\partial U}\right)\right]_{\mathrm{eq}} \\ \boldsymbol{C} &= \left[\frac{\partial Y}{\partial\mathbb{X}}\right]_{\mathrm{eq}} \end{aligned}$$

1) Moving Mass Servo Design: The first objective is to choose an input $u_{\mathrm{p}} \in \{u_{\mathrm{p}_x}, u_{\mathrm{p}_y}\}$ such that the position of the longitudinal moving mass $r_{\mathrm{p}} \in \{r_{\mathrm{p}_x}, r_{\mathrm{p}_y}\}$ asymptotically tracks a desired trajectory $r_{\mathrm{p_d}} \in \{r_{\mathrm{p}_{x_{\mathrm{d}}}}, r_{\mathrm{p}_{y_{\mathrm{d}}}}\}$. With $U = u_{\mathrm{p}}$ and $Y = r_{\mathrm{p}}$ in equations (7) and (8), the scalar $\boldsymbol{CAB}$ is nonzero. One may choose

$$u_{\mathrm{p}} = \frac{1}{\mathbf{CAB}}(\ddot{r}_{\mathrm{p}} - \mathbf{CA}^2\triangle\mathbb{X} + [\omega_{\mathrm{n}}^2 \;\; 2\zeta\omega_{\mathrm{n}}]\mathbf{e})$$

where $\mathbf{e} = [e, \dot{e}]^T$ and $e = r_{\mathrm{p_d}} - r_{\mathrm{p}}$ and where $\omega_{\mathrm{n}} \in \{\omega_{\mathrm{n}_x}, \omega_{\mathrm{n}_y}\}$ and $\zeta \in \{\zeta_x, \zeta_y\}$ are control parameters. The trajectory tracking control law requires that the reference trajectory $r_{\mathrm{p_d}}$ be twice differentiable. To ensure this, we define a linear reference model with the same relative degree. Let $\mathbf{r}_{\mathrm{p_d}} = [r_{\mathrm{p_d}}, \dot{r}_{\mathrm{p_d}}]^T$ and define, for each servoactuator, the reference model dynamics

$$\begin{aligned} \dot{\mathbf{z}} &= \begin{pmatrix} 0 & 1 \\ -\omega_{\mathrm{r}}^2 & -2\zeta_{\mathrm{r}}\omega_{\mathrm{r}} \end{pmatrix}\mathbf{z} + \begin{pmatrix} 0 \\ \omega_{\mathrm{r}}^2 \end{pmatrix} r(t) \\ r_{\mathrm{p_d}} &= \begin{pmatrix} 1 & 0 \end{pmatrix}\mathbf{z} \end{aligned}$$

where $r(t) \in \{r_x(t), r_y(t)\}$ is the (possibly discontinuous) reference command to be filtered. The reference model parameters may be chosen to accommodate magnitude and rate limits on the moving mass actuator. In physical implementations, the servo-actuation system is self-contained and there is no need for controller design. We include this element explicitly, though, in order to account for the full complexity of the multi-body mechanical system model, and in order to allow careful study of issues such as actuator magnitude and rate saturation which are important effects for underwater gliders.

2) Buoyancy Control Design: Next, we design an input u_{b} such that the net mass $\tilde{m}$ asymptotically tracks a desired value $\tilde{m}_{\mathrm{d}}$. The simplest approach is to choose

$$u_{\mathrm{b}} = -k_{\mathrm{b}}\left(\tilde{m} - \tilde{m}_{\mathrm{d}}\right)$$

where the constant k_{b} is chosen to accommodate the rate limit on u_{b}.

B. Feedback Control Design

The objective here is to design single-input, single-output PID control loops to control the vehicle speed V, glide path angle γ, and heading rate $\dot{\psi}$. Let $G(s)$ represent the transfer function for a particular control channel and let $G_{\mathrm{c}}(s)$ represent the PID controller:

$$G_c(s) = K_p(1 + \frac{1}{T_i s} + T_d s)$$

The proportional gain K_p, the integrator time T_i and the derivative time T_d are parameters to be tuned by the control designer. In the time domain, the control signal is

$$u(t) = K_p e + K_i \int_{t_0}^{t} e(\tau)d\tau + K_d\dot{e}$$

where $K_i = K_p/T_i$ and $K_d = K_p T_d$. The error signal $e(t)$ measures the difference between the actual and commanded value of the output. Speed and glide path angle are inherently coupled for underwater gliders, just as they are for airplanes. For a *fixed* glide path angle, speed can be directly modulated by changing the net mass $\tilde{m}$. However, changing $\tilde{m}$ requires pressure-volume work which is relatively expensive, especially at depth. In practice, it is best to modulate $\tilde{m}$ as infrequently as possible. Here, we focus on controlling the glide path angle γ by modulating the longitudinal moving mass position $r_{\mathrm{p_x}}$. Let $e_\gamma(t) = \gamma_{\mathrm{d}} - \gamma(t)$, where $\gamma_{\mathrm{d}} = \gamma_0$ is the nominal value of the glide path angle as computed

for wings-level equilibrium flight. The longitudinal moving mass reference signal is

$$r_{\mathrm{x}} = K_{p_\gamma} e_\gamma + K_{i_\gamma} \int_{t_0}^{t} e_\gamma(\tau) d\tau + K_{d_\gamma} \dot{e}_\gamma.$$

The channel from lateral mass position $r_{\mathrm{p_y}}$ to turn rate $\dot{\psi}$ is non-minimum phase, with a single zero in the right half plane. In principle, this non-minimum phase zero limits performance (closed-loop bandwidth). In practice, though, closing the loop from turn rate to lateral mass location is quite effective, provided the performance limitations are acknowledged in control parameter selection. Let $e_{\dot{\psi}}(t) = \dot{\psi}_{\mathrm{d}} - \dot{\psi}(t)$, where $\dot{\psi}_{\mathrm{d}}$ is the desired turn rate. The lateral moving mass control signal is

$$r_{\mathrm{y}} = K_{p_{\dot{\psi}}} e_{\dot{\psi}} + K_{i_{\dot{\psi}}} \int_{t_0}^{t} e_{\dot{\psi}}(\tau) d\tau + K_{d_{\dot{\psi}}} \dot{e}_{\dot{\psi}}.$$

With the glide path and turn rate PID controllers so defined, the first step is to tune these controllers for the linearized system dynamics. Having done so, the next step is to re-tune the controllers as necessary for the nonlinear dynamics through simulation.

VI. SIMULATION RESULTS

A reasonably sophisticated model of the *Slocum* glider given in [1] was linearized about the following equilibrium flight condition, which corresponds to wings-level, descending flight:

$$V_0 = 0.77 \text{ m/s}, \qquad \alpha_0 = 4.3^\circ, \qquad \theta_0 = -8.4^\circ,$$
$$\gamma_0 = -12.7^\circ \qquad \text{and} \qquad \tilde{m}_0 = 0.63 \text{ kg}.$$

The moving mass values are $m_{\mathrm{p_x}} = m_{\mathrm{p_y}} = 9$ kg. The servo-actuator parameter values are

$$\omega_{\mathrm{n_x}} = 20 \text{ rad/s} \quad \zeta_{\mathrm{x}} = 0.001 \quad \omega_{\mathrm{r_x}} = 0.8 \text{ rad/s} \quad \zeta_{\mathrm{r_x}} = 1$$
$$\omega_{\mathrm{n_y}} = 20 \text{ rad/s} \quad \zeta_{\mathrm{y}} = 0.01 \quad \omega_{\mathrm{r_y}} = 0.8 \text{ rad/s} \quad \zeta_{\mathrm{r_y}} = 1$$

The PID control parameter values are

$$K_{p_\gamma} = -0.5 \text{ m} \qquad T_{i_\gamma} = 2.3 \text{ s} \qquad T_{d_\gamma} = 2 \text{ s}$$
$$K_{p_{\dot{\psi}}} = 0.2 \text{ m/(rad/s)} \qquad T_{i_{\dot{\psi}}} = 0.65 \text{ s} \qquad T_{d_{\dot{\psi}}} = 0.39 \text{ s}$$

Figures 3 through 7 compare the results of simulations using open- and closed-loop control. Figure 3 shows the lateral mass location in response to a command sequence that is intended to effect a right turn, a straight segment, and left turn (viewed from above). In the open-loop case, the moving mass is simply commanded to move to the (approximate) equilibrium value corresponding to a desired heading rate $\dot{\psi}_{\mathrm{d}}$. In the closed-loop case, however, the heading rate is directly commanded, with the lateral moving mass actuator responding as necessary. The resulting path is depicted in Figure 4. This path is reminiscent of a Dubins path, although the vehicle and actuator dynamics effectively result in a turn *acceleration* limit, in addition to the assumed turn rate limit. Time-optimal paths for a Dubins car with acceleration limits are discussed in [8] and [10], where it is recognized that extremal paths comprise sequences of straight, clothoidal, and circular segments. In reference to these results, we call such paths "suboptimal Dubins paths."

Figures 5 and 6 show desired, open-loop, and closed-loop value of the vehicle's glide path angle and turn rate. As expected, the deviation between the open-loop values and the desired values is significant. In Figure 6, the small spikes at the end of each segment likely correspond to reaction forces due to the movement of the lateral mass within the vehicle. We note that the turn rate magnitudes are of the same order as turn rates seen in glider operations. The *Slocum* glider, for example, can achieve a 20-30 meter turn radius at speeds on

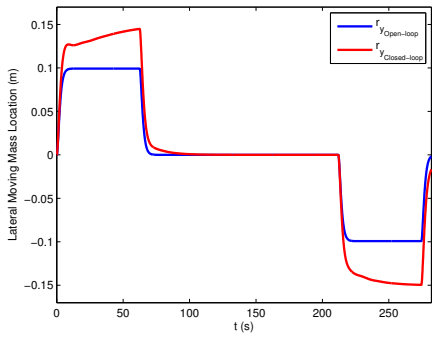

Fig. 3. Lateral moving mass location (open- and closed-loop).

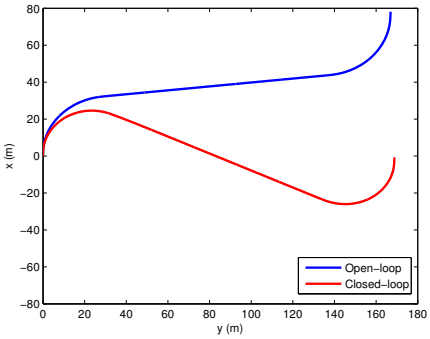

Fig. 4. *Slocum* path in response to command sequence.

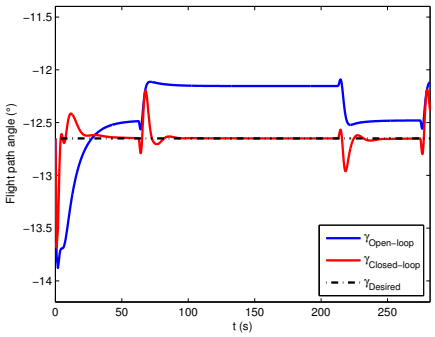

Fig. 5. Glide path angle response to command sequence.

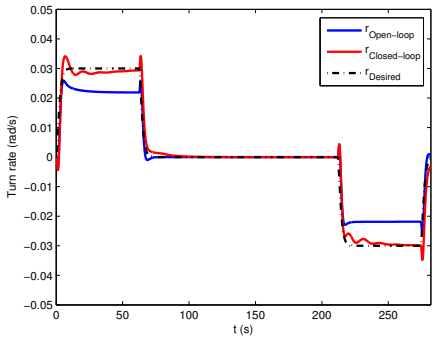

Fig. 6. Turn rate response to command sequence.

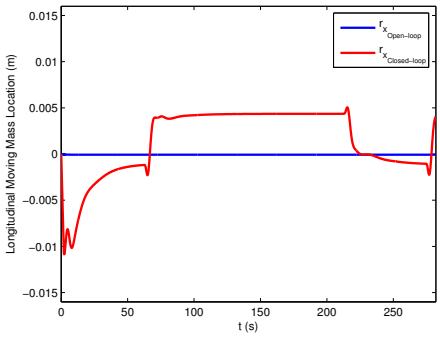

Fig. 7. Variation in longitudinal moving mass position from nominal.

the order of half a meter per second. A shallow-water variant of *Slocum*, which includes a movable rudder, can perform turns with a 7 meter radius [2]. Figure 7 shows the location of the longitudinal moving mass, which must move in order to regulate the glide path angle.

It must be stressed that the final guidance loop has not been closed, at this point. That is, we have not developed a control law to make the vehicle track a commanded *path*, such as a suboptimal Dubins path. Rather, we have designed the underlying motion control system over which a guidance loop might be imposed.

VII. CONCLUSIONS AND FUTURE WORK

A multi-body dynamic model was developed for an underwater glider that includes both longitudinal and lateral actuators as well as the buoyancy actuator. Building on prior results in glider steady motion analysis, a motion control system was developed to control glide path angle and turn rate. The control system includes model reference controllers for the servo-actuators, to allow saturation effects to be easily incorporated. The glide path angle and turn rate controllers are single-input, single-output PID loops. The control parameters were tuned using a nonlinear simulation that includes actuator magnitude and rate limits. The controller's effectiveness was demonstrated in simulation. Although the motion control system developed here allows one to implement general guidance strategies, our aim is to enable closed-loop tracking of time-suboptimal glider paths that can be generated in real time using existing results for nonholonomic mobile robots. These Dubins-like paths accommodate turn rate and turn acceleration limits, which are essential aspects of underwater glider motion. For underwater gliders travelling at constant speed and maximum flight efficiency, minimum arclength paths are minimum energy paths. Closed-loop guidance, such as a line-of-sight strategy, is required because only approximate solutions for steady turning motion are available and because model and environmental uncertainty is inevitable. The motion control system developed here is a necessary step toward convergent path following.

Acknowledgements. This work was supported by the Office of Naval Research under grant number N00014-08-1-0012. The authors gratefully acknowledge the input of the anonymous reviewers.

REFERENCES

[1] P. Bhatta. *Nonlinear Stability and Control of Gliding Vehicles*. PhD thesis, Princeton University, 2006.

[2] R. E. Davis, C. C. Eriksen, and C. P. Jones. Autonomous buoyancy-driven underwater gliders. In G. Griffiths, editor, *Technology and Applications of Autonomous Underwater Vehicles*, volume 2, chapter 3. Taylor and Francis, 2002.

[3] L. E. Dubins. On curves of minimal length with a constraint on average curvature and with prescribed initial and terminal positions and tangents. *American Journal of Mathematics*, 79, 1957.

[4] C. C. Eriksen, T. J. Osse, R. D. Light, T. Wen, T. W. Lehman, P. L. Sabin, J. W. Ballard, and A. M. Chiodi. Seaglider: A long-range autonomous underwater vehicle for oceanographic research. *Journal of Oceanic Engineering*, 26(4):424–436, 2001. Special Issue on Autonomous Ocean-Sampling Networks.

[5] J. S. Geisbert. Hydrodynamic modeling for autonomous underwater vehicles using computational and semi-empirical methods. Master's thesis, Virginia Polytechnic Institute and State University, 2007.

[6] J. G. Graver, J. Liu, C. A. Woolsey, and N. E. Leonard. Design and analysis of an underwater glider for controlled gliding. In *Conference on Information Sciences and Systems*, pages 801–806, 1998.

[7] J. Guckenheimer and P. Holmes. *Nonlinear Oscillations, Dynamical Systems, and Bifurcations of Vector Fields*. Springer-Verlag, New York, NY, 1983.

[8] V. Kostov and E. Degtiariova-Kostova. Suboptimal paths in the problem of a planar motion with bounded derivative of the curvature. Technical Report 2051, Institut National de Recherche en Informatique et en Automatique (INRIA), July 1993.

[9] N. Mahmoudian, C. Woolsey, and J. Geisbert. Steady turns and optimal path for underwater gliders. Hilton Head, SC, Aug 20-23 2007. AIAA Guidance, Navigation and Control Conference and Exhibit.

[10] A. Scheuer and Ch. Laugier. Planning sub-optimal and continuous-curvature paths for car-like robots. In *IEEE/RSJ International Conference on Intelligent Robots and Systems*, pages 25–31, Victoria, B.C., Canada, October 1998.

[11] J. Sherman, R. E. Davis, W. B. Owens, and J. Valdes. The autonomous underwater glider "Spray". *Journal of Oceanic Engineering*, 26(4):437–446, 2001. Special Issue on Autonomous Ocean-Sampling Networks.

[12] H. J. Sussmann and G. Tang. Shortest paths for the Reeds-Shepp car: A worked out example of the use of geometric techniques in nonlinear optimal control. Technical Report 91-10, Rutgers University Center for Systems and Control, New Brunswick, NJ, 1991.

[13] D. C. Webb, P. J. Simonetti, and C. P. Jones. SLOCUM: An underwater glider propelled by environmental energy. *Journal of Oceanic Engineering*, 26(4):447–452, 2001. Special Issue on Autonomous Ocean-Sampling Networks.

[14] C. A. Woolsey. Reduced Hamiltonian dynamics for a rigid body/mass particle system. *Journal of Guidance, Control, and Dynamics*, 28(1):131–138, January-February 2005.